Adaptive Receive Processing of Spatially-Modulated Physical Radar Emissions

Patrick M. McCormick*, *Student Member, IEEE*, Thomas Higgins, *Member, IEEE*, Shannon D. Blunt, *Senior Member, IEEE,* and Muralidhar Rangaswamy, *Fellow, IEEE*

***Abstract*—Inspired by the fixational movements of the human eye, fast-time spatial modulation was recently demonstrated as a particular physically-realizable form of a multiple-input multiple-output (MIMO) radar emission. The attendant coupling of the delay and angle dimensions has been shown to provide a modest improvement in spatial separation, even when using non-adaptive pulse compression and beamforming. Here this continuous emission paradigm is appropriately discretized and a joint delay-angle adaptive filtering strategy is developed that exploits the physical waveform-diverse emission structure to realize significant enhancement in target separability.**

***Index Terms*— adaptive filtering, MIMO radar, waveform diversity**

I. Introduction

In [1,2] the waveform-diverse array (WDA) emission structure was developed which subsumes the frequency-diverse array (FDA) framework [3-7] for pulsed radar. The WDA scheme leverages the recent development of physically-realizable polyphase-coded frequency modulated (PCFM) waveforms [8,9] that is based on continuous phase modulation (CPM), commonly employed for aeronautical telemetry [10], deep-space communications [11], and the Bluetooth™ wireless standard [12]. The WDA structure was inspired by the biological process of the human eye (and of other animals possessing fovea) known as *fixational eye movement* in which the eye performs slow movements known as *drift* and rapid movements known as *microsaccades* [13,14]. The current scientific consensus is that such movements enhance contrast and aid in resolving spatial ambiguities. There is even evidence [15] that these eye movements adapt according to environmental conditions (e.g. amount of lighting) and the active attention of the observer, thus suggesting a connection to cognitive sensing [16] within the visual cortex for this waveform-diverse emission paradigm [17-19].

The WDA was a step towards mimicking the passive sensing behavior of the eye within the active sensing paradigm of radar. It was demonstrated in [1,2] that, using only standard (non-adaptive) pulse compression and beamforming, spatial resolution and target discrimination could be enhanced by as much as 30%, albeit with a commensurate trade-off in range resolution as a result of spreading the illuminating waveform across a band of spatial angles. It is worth noting that WDA represents a special case of MIMO radar that maintains a focused mainbeam (at least at each instant in time during the pulse) and is physically realizable for a high-power radar having arbitrary waveform generation capability at each antenna element. It was also observed in [2] that the "goodness" of a particular WDA delay-angle emission is dependent on the underlying waveform and the specific nature of the spatial modulation. For example, use of a linear frequency modulated (LFM) chirp combined with relatively linear intra-pulse spatial steering provides what amounts to a tapering effect in the range domain that realizes significant range sidelobe suppression (with the associated range resolution degradation as well). It was also found that intra-pulse beamsteering exceeding the nominal beamwidth of the array yielded lost signal-to-noise ratio (SNR) without any compensating improvement in spatial resolution. Thus, like the eye, it is desirable for the WDA to maintain sufficient spatial focus on target (or set of proximate targets).

Where [1,2] focused on the physical emission structure of WDA, here we consider how joint adaptive delay-angle receive processing can exploit this coupled emission, since dimensional coupling is known in general to provide a multiplicative increase in degrees of freedom (Space-Time Adaptive Processing (STAP) being a prominent example of such in radar). To accomplish this goal, two separate adaptive approaches for pulse compression and beamforming are unified, along with necessary measures to address the physical nature of the emission. Specifically, the Adaptive Pulse Compression (APC) algorithm was developed using reiterative minimum mean-square error (RMMSE) estimation to suppress range sidelobes generated by radar codes [20] and has recently been generalized for application to arbitrary FM waveforms [21]. The same underlying RMMSE approach was likewise used to develop the Re-Iterative Super-Resolution (RISR) algorithm [22] for adaptive beamforming that also inherently

This work was supported in part by the U.S. Air Force Office of Scientific Research and the Radar Division of the U.S. Naval Research Laboratory.

Patrick M. McCormick is with the Electrical Engineering & Computer Science Department, University of Kansas, 1520 W. 15th St., Lawrence, KS, 66045 USA (e-mail: pmccormick@ittc.ku.edu)

Thomas Higgins is with the Naval Research Laboratory – Radar Division, Building 60, 4555 Overlook Ave. SW, Washington D.C., 20375 USA (e-mail: Thomas.Higgins@nrl.navy.mil)

Shannon D. Blunt is with the Electrical Engineering & Computer Science Department, University of Kansas, 1520 W. 15th St., Lawrence, KS, 66045 USA (e-mail: sdblunt@ittc.ku.edu)

Muralidhar Rangaswamy is with the Air Force Research Lab – Sensors Directorate, Building 620, 2241 Avionics Circle, Wright-Patterson AFB, OH, 45433 USA (e-mail: muralidhar.rangaswamy@us.af.mil).

permits the inclusion of calibration uncertainty. Because they are based on the same estimation framework, it is shown that a coupled delay-angle estimator denoted as Space-Range Adaptive Processing (SRAP) can be obtained that is applicable to such coupled emission schemes (i.e. MIMO).

II. Waveform-Diverse Array

The formulation for the WDA was derived in [1,2]. Here the derivation is briefly reprised to illustrate the linkage between the joint delay-angle emission and subsequent adaptive receive processing. In particular, the impact of sampling must be considered since the emission is, in theory, not bandlimited (though good spectral roll-off is achieved [8]) and to address straddling effects in range and angle (also known as the "off-grid" problem).

While the WDA concept is applicable to any array geometry, the following is based on the assumption of a uniform linear array (ULA). The array element spacing is denoted as d with spatial angle θ defined relative to array boresight (where $\theta = 0°$). It is assumed that emitted/received signals satisfy the array narrowband assumption and thus the associated electrical angle is $\widehat{\theta} = 2\pi d \sin(\theta)/\lambda$, with λ the wavelength associated with the carrier frequency.

A. WDA Definition

The waveform diverse array (WDA) concept necessitates a dedicated waveform generator at each antenna element. We consider physical waveforms that are amenable to high-power transmitters and thus restrict attention to the class of polyphase-coded FM (PCFM) waveforms (Fig. 1) [8,9] that are enabled by a continuous phase modulation (CPM) implementation, and thus are constant modulus and differentiable (i.e. continuous).

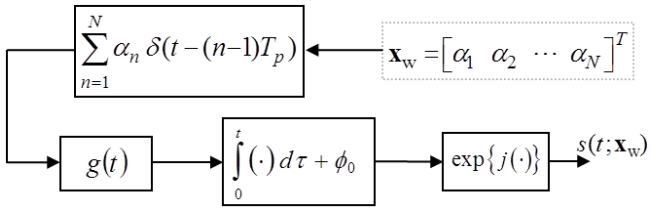

Fig. 1. Polyphase-coded FM (PCFM) waveforms implementation using waveform code $\mathbf{x}_{\mathrm{w}}$ [8]

Given a traditional polyphase radar code with $N+1$ chip phase values $\phi_0, \phi_1, \cdots, \phi_N$, a train of N impulses with time separation T_p are formed such that the total pulsewidth is $T = NT_p$. The nth impulse is weighted by α_n, which is the phase change between successive chips of the polyphase code as determined by

$$\alpha_n = \begin{cases} \tilde{\alpha}_n & \text{if } |\tilde{\alpha}_n| \le \pi \\ \tilde{\alpha}_n - 2\pi \operatorname{sgn}(\tilde{\alpha}_n) & \text{if } |\tilde{\alpha}_n| > \pi \end{cases}, \tag{1}$$

where

$$\tilde{\alpha}_n = \phi_n - \phi_{n-1} \quad \text{for} \quad n = 1, \cdots, N, \tag{2}$$

and sgn(•) is the signum operation. The shaping filter $g(t)$ may, for example, be rectangular (RECT) or raised cosine (RC) with the requirements 1) that it integrates to unity over the real line; and 2) that it has time support on $[0, T_p]$. Per Fig. 1, the PCFM waveform is thus defined as [8]

$$s(t;\mathbf{x}_{\mathrm{w}}) = \exp\left\{ j \left(\int_0^t g(\tau) * \left[\sum_{n=1}^{N} \alpha_n \, \delta\left(\tau - (n-1)T_p\right) \right] d\tau + \phi_0 \right) \right\}, \tag{3}$$

where $*$ denotes convolution, ϕ_0 is the initial phase value of the code, and the sequence of phase changes are collected into the vector $\mathbf{x}_{\mathrm{w}} = [\alpha_1 \;\; \alpha_2 \;\; \cdots \;\; \alpha_N]^T$ that parameterizes the complex baseband waveform. If the phase change values in the waveform code adequately cover the interval $[-\pi, \pi]$, then the dimensionality of $\mathbf{x}_{\mathrm{w}}$ is a good approximation to the time bandwidth product of the continuous waveform $s(t;\mathbf{x}_{\mathrm{w}})$.

In [2] this physical waveform implementation was extended to likewise parameterize physically a form of fast-time spatial modulation during the pulse by controlling the relative phases across the antenna array. Here a set of $N+1$ values $\Delta_0, \Delta_1, \cdots, \Delta_N$ is defined as a sequence of spatial angle offsets relative to center direction θ_{C}. The subsequent spatial phase-change sequence (as a function of code index *n*) for use with the PCFM implementation and a uniform linear array is

$$\varepsilon_n = \frac{2\pi d}{\lambda}\left(\sin(\theta_{\mathrm{C}} + \Delta_n) - \sin(\theta_{\mathrm{C}} + \Delta_{n-1}) \right) \text{ for } n = 1, \cdots, N, \tag{4}$$

noting that each Δ_n can be positive or negative. It shall be assumed that the values of Δ_n are sufficiently small to avoid steering the beam beyond the endfire direction and thereby inducing a spatial wrap-around effect. With a structure similar to (3), the spatial phase modulation as a function of continuous time is represented as

$$b(t;\mathbf{x}_{\mathrm{s}}) = \exp\left\{ -j \left(\int_0^t g(\tau) * \left[\sum_{n=1}^{N} \varepsilon_n \, \delta\left(\tau - (n-1)T_p\right) \right] d\tau + \widehat{\Delta}_0 \right) \right\} \tag{5}$$

where the sequence of spatial phase changes from (4) are collected in the spatial modulation code $\mathbf{x}_{\mathrm{s}} = [\varepsilon_1 \;\; \varepsilon_2 \;\; \cdots \;\; \varepsilon_N]^T$ and

$$\widehat{\Delta}_0 = \frac{2\pi d}{\lambda} \sin\left(\theta_{\mathrm{C}} + \Delta_0\right) \tag{6}$$

is the initial electrical angle. The leading negative sign of the spatial modulation in (5), relative to the waveform modulation of (3), reflects the phase delay compensation for spatial beamsteering on transmit.

The signal generated by the mth antenna element is thus

$$s_m(t, \theta_{\mathrm{C}}; \mathbf{x}_{\mathrm{w}}, \mathbf{x}_{\mathrm{s}}) = \frac{1}{\sqrt{T}} s(t;\mathbf{x}_{\mathrm{w}}) \, b^m(t;\mathbf{x}_{\mathrm{s}}), \tag{7}$$

where the normalization term provides unit transmit energy

per antenna element. The Vandermonde-like form $(\bullet)^m$ across the uniform linear array yields, from (7),

$$b^m(t;\mathbf{x}_S)=\exp\left\{-jm\left(\int_0^t g(\tau)*\left[\sum_{n=1}^{N}\varepsilon_n\,\delta\left(\tau-(n-1)T_p\right)\right]d\tau+\hat{\Delta}_0\right)\right\} \tag{8}$$

for $m=-(M-1)/2,\ -(M-1)/2+1,\ \ldots,\ (M-1)/2$. As discussed in [2], the array is defined such that index $m=0$ is in the center of the array for the notational convenience of symmetry.

In the case of no spatial modulation, the set of spatial offsets are $\Delta_0=\Delta_1=\cdots=\Delta_N=0$, such that the resulting N phase changes are likewise $\varepsilon_1=\varepsilon_2=\cdots=\varepsilon_N=0$. As a result, (8) simplifies to $b^m(t;\mathbf{x}_S)=\exp\{-jm\hat{\Delta}_0\}$, which is simply the phase delay on the *m*th antenna element needed to steer a stationary beam in the direction of spatial angle θ_C, thus realizing standard beamforming.

Combining (3) and (8) into a single per-element emission yields

$$s_m(t,\theta_C;\mathbf{x}_W,\mathbf{x}_S)=\frac{1}{\sqrt{T}}\exp\left\{j\left(\int_0^t g(\tau)*\left[\sum_{n=1}^{N}\alpha_{n,m}\,\delta\left(\tau-(n-1)T_p\right)\right]d\tau+\phi_{0,m}\right)\right\} \tag{9}$$

where $\alpha_{n,m}=(\alpha_n-m\varepsilon_n)$ is the joint waveform/spatial code for the *m*th element and $\phi_{0,m}=(\phi_0-m\hat{\Delta}_0)$ is the joint initial phase for the *m*th element. Care must be taken to avoid extending the instantaneous phase difference between emissions generated by adjacent antenna elements to the point where the array radiates into "imaginary" or "invisible" space, which could cause severe damage to the radar [23]. Such an event occurs when the instantaneous element spacing is less than $\lambda/2$ for any wavelength corresponding to the upconverted bandwidth of the emission and the mainlobe is steered towards or near endfire. Thus, a portion of the emission is no longer radiated but stored in the near field due to a dominant reactive component of the array impedance and can result in damage to the transmitter [24]. Such an effect does not occur if the spatial angle spread is kept sufficiently small (e.g. not exceeding the first-null beamwidth with respect to θ_C).

B. Far-Field WDA Emission

An accurate assessment of the far-field emission requires incorporation of array mutual coupling and calibration effects (to the degree known). Such knowledge is particularly important for MIMO radar since the intrinsic coupling of delay and angle subsequently couples the waveforms to these antenna effects [25,26]. We shall not address these effects here but they may be readily inserted as available.

A composite far-field emission for time *t* and spatial angle θ can be expressed as

$$g(t,\theta,\theta_C)=\frac{1}{M}\sum_{m=-(M-1)/2}^{(M-1)/2}s_m(t,\theta_C)\,e^{jm\,2\pi d\sin(\theta)/\lambda}, \tag{10}$$

where $s_m(t,\theta_C)$ is taken from (9) and the exponential term is the delay resulting from path length differences as a function of angle θ. Note that the dependence on the waveform code $\mathbf{x}_W$ and spatial modulation code $\mathbf{x}_S$ have been suppressed for brevity. Using (10), a time-varying beampattern (TVBP) can be defined as

$$B_{TV}(t,\theta,\theta_C)=g(t,\theta,\theta_C)\,g^*(t,\theta,\theta_C) \tag{11}$$

for $0\le t\le T$, where $(\bullet)^*$ denotes complex conjugation. The TVBP thus allows for a view of the instantaneous spatial attributes of the emission as a function of time over the pulsewidth *T*.

On receive, the reflected signal incident upon the *m*th antenna element can be expressed as

$$y_m(t,\theta_C)=\int\left[x(t,\theta)*g(t,\theta,\theta_C)\,e^{jm\,2\pi d\sin(\theta)/\lambda}\right]d\theta+u(t), \tag{12}$$

where $x(t,\theta)$ is the complex scattering as a function of time (delay) and spatial angle. Receive beamforming (for spatial angle β) and pulse compression can be represented as

$$z(t,\beta,\theta_C)=\frac{1}{M}\sum_{m=-(M-1)/2}^{(M-1)/2}y_m(t,\theta_C)\,e^{-jm\,2\pi d\sin(\beta)/\lambda} \tag{13}$$

and

$$\hat{x}(\tau,\beta,\theta_C)=\int z(t,\theta,\theta_C)\,h^*(t-\tau,\beta,\theta_C)\,dt, \tag{14}$$

respectively. In (14), $h(t,\beta,\theta_C)$ is the pulse compression filter for the incident signal from spatial angle β and is a function of the far-field emission $g(t,\beta,\theta_C)$ in that same angle. Due to the modulation of the mainbeam (and sidelobes) on transmit, the emission in any given spatial direction is amplitude modulated and thus the power is spread unevenly in space. Therefore, it is useful to normalize the angle-dependent filters to unity gain to avoid artificially scaling the estimated scattering response. As such, we define a unity-gain normalized matched filter as

$$h(t,\beta,\theta_C)=\frac{g(t,\beta,\theta_C)}{\left[\int_0^T g(t,\beta,\theta_C)\,g^*(t,\beta,\theta_C)\,dt\right]^{1/2}} \tag{15}$$

so that (14) actually yields the illumination-scaled response

$$\hat{\hat{x}}(\tau,\beta,\theta_C)=\hat{x}(\tau,\beta,\theta_C)\left[\int_0^T g(t,\beta,\theta_C)\,g^*(t,\beta,\theta_C)\,dt\right]^{1/2}. \tag{16}$$

In [2] it was shown that enhanced separability of proximate targets was enabled through this coupled delay-angle emission using standard non-adaptive beamforming and pulse compression of (13) and (14), respectively. However, it is well known that such coupling induces a multiplicative increase in degrees of freedom. As such, we now consider how to realize (13)-(16) with a filter that is jointly adaptive in delay and angle.

III. Joint Adaptive Processing in Delay-Angle

Here the Space-Range Adaptive Processing (SRAP) algorithm is developed for application to the above physical delay-angle coupled emission. It should be noted that the SRAP algorithm is applicable to any physically realizable MIMO emission, though in this paper we shall limit attention to the WDA structure, which is expected to be more robust to imperfect array calibration and mutual calibration by virtue of forming a coherent beam (that moves during the pulsewidth).

The SRAP algorithm extends the recursive MMSE-based approach previously employed to perform adaptive pulse compression [20] and direction of arrival estimation [22] to a joint delay-angle framework in which a unique receive filter is adaptively determined for each range-angle cell. A preliminary instantiation of SRAP was presented in [27], albeit for an emission scheme that lacks the physical attributes of the WDA scheme described above.

To derive a joint delay-angle filter structure it is first necessary to define discretized versions of the continuous emission and received signal model described in Section II. We then consider the impact of this discretization on the subsequent adaptive filtering.

A. Discretized Signal Model

The waveforms $s_m(t,\theta_{\rm C})$ from (9), transmitted from the M elements of a uniform linear array, can be collectively represented in a discretized manner as the $KN\times M$ matrix $\mathbf{S}(\theta_{\rm C})$. The mth column of this matrix contains the length-KN discretized waveform $\mathbf{s}_m(\theta_{\rm C})$ associated with the mth element of the array. For standard beamforming the columns of $\mathbf{S}(\theta_{\rm C})$ are identical aside from the phase shift for spatial beamforming in direction $\theta_{\rm C}$.

Recall that N is the length of the waveform code $\mathbf{x}_{\rm w}$ and that it approximates the time-bandwidth product of the waveform. The scalar K ($\geq$1) is the amount of "over-sampling" relative to the 3-dB bandwidth of $s_m(t,\theta_{\rm C})$, noting that true over-sampling is not possible since a pulsed emission is not bandlimited in theory. Increasing K reduces the effect of range straddling (or cusping) effects for pulse compression [8, 21], though doing so also increases the computation cost (due to higher dimensionality) and could lead to ill-conditioning effects for adaptive processing. Some degree of such "over-sampling" is necessary to obtain a sufficiently high-fidelity representation of the received signal to permit accurate receive estimation and we shall discuss an appropriate way in which to contend with the deleterious effects that subsequently arise.

Again using the center of the array as reference, define the spatial steering vector associated with electrical angle $\hat{\theta}$ as

$$\mathbf{v}_\theta = e^{-j[(M-1)/2]\hat{\theta}}\left[\begin{array}{ccccc}1 & e^{j\hat{\theta}} & e^{j2\hat{\theta}} & \cdots & e^{j(M-1)\hat{\theta}}\end{array}\right]^T \quad (17)$$

with $(\bullet)^T$ the transpose operation. A discretized version of the far-field emission $g(t,\theta,\theta_{\rm C})$ from (10) can thus be expressed as the column vector

$$\mathbf{g}(\theta,\theta_{\rm C}) = \frac{1}{M}\,\mathbf{S}(\theta_{\rm C})\,\mathbf{v}_\theta\,. \quad (18)$$

For convenience we shall henceforth suppress the inherent dependence on the center look direction $\theta_{\rm C}$ so that the emission structure in (18) is expressed simply as $\mathbf{g}(\theta)$.

By discretization of (12) and expansion to M antenna elements, the response at the array from a single far-field scatterer in spatial direction θ can be written as a complex scaling of the matrix $\mathbf{g}(\theta)\mathbf{v}_\theta^T$, the mth column of which corresponds to the reflected far-field emission that is received by the mth antenna element. Therefore, at a given discrete time delay ℓ the incident response upon the array can be approximated as the length M row vector

$$\mathbf{y}_{\rm disc}(\ell) = \sum_\theta \mathbf{x}^T(\ell,\theta)\;\mathbf{g}(\theta)\,\mathbf{v}_\theta^T + \mathbf{u}_{\rm disc}(\ell)\,. \quad (19)$$

In (19), $\mathbf{x}(\ell,\theta) = [x(\ell,\theta)\;\; x(\ell-1,\theta)\;\cdots\; x(\ell-KN+1,\theta)]^T$ is a contiguous collection of discretized complex scattering coefficients in range corresponding to angle θ with which the associated far-field emission convolves at delay ℓ, and $\mathbf{u}_{\rm disc}(\ell)$ is a $1\times M$ vector of complex additive noise samples. The representation in (19) is an approximation because true Nyquist sampling cannot be achieved for pulsed radar echoes, though the physical emissions based on PCFM waveforms do provide excellent spectral roll-off [8]. For such waveforms the pulse rise/fall-time becomes the limiting factor with regard to spectral containment [28].

The collection of KN contiguous fast-time snapshots of (19) can be expressed as the $KN\times M$ matrix

$$\mathbf{Y}(\ell) = \sum_\theta \mathbf{X}(\ell,\theta)\,\mathbf{g}(\theta)\,\mathbf{v}_\theta^T + \mathbf{U}(\ell)\,, \quad (20)$$

where

$$\mathbf{X}(\ell,\theta) = \left[\begin{array}{cccc} x(\ell,\theta) & x(\ell-1,\theta) & \cdots & x(\ell-KN+1,\theta) \\ x(\ell+1,\theta) & x(\ell,\theta) & \cdots & x(\ell-KN+2,\theta) \\ \vdots & \vdots & \ddots & \vdots \\ x(\ell+KN-1,\theta) & x(\ell+KN-2,\theta) & \cdots & x(\ell,\theta) \end{array}\right] \quad (21)$$

is a $KN\times KN$ matrix containing $x(\ell,\theta)$ and the $2KN-2$ surrounding range cells. To make the received signal model amenable for joint delay-angle processing, the $KN\times M$ matrix representation in (20) is reorganized as the $KNM\times 1$ vector

$$\mathbf{y}(\ell) = \sum_\theta \left[\mathbf{X}(\ell,\theta)\;\mathbf{g}(\theta)\right]\otimes\mathbf{v}_\theta + \mathbf{u}(\ell)\,, \quad (22)$$

where the symbol $\otimes$ denotes the Kronecker product and $\mathbf{u}(\ell) = \text{vec}[\,\mathbf{U}^T(\ell)]$.

The receive beamforming (in direction β) and unity-gain pulse compression from (13)-(16) can be jointly expressed for this discrete representation as the delay-angle matched filter

$$\mathbf{w}_{\mathrm{MF}}(\beta) = \frac{\mathbf{g}(\beta) \otimes \mathbf{v}_{\theta}}{M \left\| \mathbf{g}(\beta) \right\|}, \tag{23}$$

where $\left\| \mathbf{g}(\beta) \right\| = [\mathbf{g}^H(\beta)\, \mathbf{g}(\beta)]^{1/2}$ and with $(\bullet)^H$ the complex-conjugate transpose operation. The discrete illumination-scaled matched filter response is thus

$$\hat{\bar{x}}_{\mathrm{MF}}(\ell, \beta) = \mathbf{w}_{\mathrm{MF}}^H(\beta)\, \mathbf{y}(\ell). \tag{24}$$

As with (16), the matched filter response in (24) is an estimate of $\bar{x}(\ell, \beta) = x(\ell, \beta) \left\| \mathbf{g}(\beta) \right\|$, where $\left\| \mathbf{g}(\beta) \right\|$ is the intensity of the radar illumination that varies with spatial angle. The unity-gain pulse compression filtering defined in (15) and discretized in (23) ensures that the resulting amplitude scaling of the filter output is due to the scattering and filter correlation response, as opposed to variations in the receive filter gain as a function of spatial angle.

B. Space-Range Adaptive Processing

The recursive minimum mean-square error (RMMSE) based filtering approach was previously developed to enable adaptive pulse compression of radar codes [20] and was subsequently also demonstrated to provide adaptive beamforming that is robust to calibration errors [22] and high-resolution EEG/MEG brain imaging of measured data [29]. For radar pulse compression it has only recently been determined how this estimation scheme may be applied to continuous FM waveforms [21] which necessitates both "over-sampling" with respect to 3 dB bandwidth (as discussed above) in combination with a down-sampled (polyphase decomposed) filter structure [30] that, collectively, provide robustness to range straddling effects. This approach will here be used to facilitate the joint adaptive delay-angle receive processing of physical MIMO emissions.

For notational convenience, the angle-dependent adaptive filters will now be expressed in terms of electrical angle $\hat{\beta}$ according to the well-known relation

$$\hat{\beta} = \frac{2\pi d}{\lambda} \sin(\beta). \tag{25}$$

Using the discretized MIMO received signal model from (22) in combination with the decomposed structure of [30], the MMSE cost function for the (scaled) complex amplitude in the range-angle cell corresponding to delay ℓ and receive electrical angle $\hat{\beta}$ is given as

$$\tilde{J}\left(\ell, \hat{\beta}\right) = \sum_{k=0}^{K-1} E\left[\left| \frac{1}{K} \bar{x}\left(\ell, \hat{\beta}\right) - \tilde{\mathbf{w}}_k^H\left(\ell, \hat{\beta}\right) \tilde{\mathbf{y}}_k(\ell) \right|^2 \right], \tag{26}$$

for down-sampling by the factor K (i.e. same as the amount of "over-sampling" with respect to 3 dB bandwidth). In (26), $E[\bullet]$ is expectation and $\tilde{\mathbf{w}}_k(\ell, \hat{\beta})$ is the kth length-NM down-sampled adaptive filter for the $(\ell, \hat{\beta})$ range-angle cell. Further,

$$\tilde{\mathbf{y}}_k(\ell) = \sum_{\theta} \left[\tilde{\bar{\mathbf{X}}}_k\left(\ell, \hat{\theta}\right) \bar{\mathbf{g}}\left(\hat{\theta}\right) \right] \otimes \mathbf{v}_{\hat{\theta}} + \tilde{\mathbf{u}}_k(\ell) \tag{27}$$

is the kth length-NM down-sampled version of the received signal from (22) where

$$\tilde{\bar{\mathbf{X}}}_k\left(\ell, \hat{\theta}\right) = \begin{bmatrix} \bar{x}\left(\ell+k, \hat{\theta}\right) & \bar{x}\left(\ell+k-1, \hat{\theta}\right) & \cdots & \bar{x}\left(\ell+k-KN+1, \hat{\theta}\right) \\ \bar{x}\left(\ell+k+K, \hat{\theta}\right) & \bar{x}\left(\ell+k+K-1, \hat{\theta}\right) & \cdots & \bar{x}\left(\ell+k-K(N-1)+1, \hat{\theta}\right) \\ \vdots & \vdots & \ddots & \vdots \\ \bar{x}\left(\ell+k+K(N-1), \hat{\theta}\right) & \bar{x}\left(\ell+k+K(N-1)-1, \hat{\theta}\right) & \cdots & \bar{x}\left(\ell+k-K+1, \hat{\theta}\right) \end{bmatrix} \tag{28}$$

is likewise the kth $N \times KN$ down-sampled version of (21). Note that the down-sampled model depicted in (27) and (28) is defined in terms of electrical angle $\hat{\theta}$ and that

$$\bar{\mathbf{g}}\left(\hat{\theta}\right) = \frac{\mathbf{g}\left(\hat{\theta}\right)}{\left\| \mathbf{g}\left(\hat{\theta}\right) \right\|} \tag{29}$$

is the unity-gain normalized far field emission so that (28) could likewise be written as $\tilde{\bar{\mathbf{X}}}_k(\ell, \hat{\theta}) = \left\| \mathbf{g}(\hat{\theta}) \right\| \tilde{\mathbf{X}}_k(\ell, \hat{\theta})$. This normalized scaling of the emissions within the received signal model prevents noise enhancement problems in the adaptive processing due to artificial compensation of scattering that received little radar illumination power.

Down-sampling is only performed in the range dimension to accommodate the need for waveform "over-sampling". Therefore, due to the Kronecker product structure involving the length M spatial steering vector $\mathbf{v}_{\hat{\theta}}$, (27) can also be expressed in the partitioned form

$$\tilde{\mathbf{y}}_k(\ell) = \begin{bmatrix} \tilde{\mathbf{y}}_{k,0} \\ \tilde{\mathbf{y}}_{k,1} \\ \vdots \\ \tilde{\mathbf{y}}_{k,N-1} \end{bmatrix} \tag{30}$$

where $\tilde{\mathbf{y}}_{k,n}(\ell)$ is the nth $M \times 1$ component that comprises the kth down-sampled receive vector. The entire $KNM \times 1$ receive signal defined in (22) can thus be shown as the collection of the interleaved down-sampled receive signals as

$$\mathbf{y}(\ell) = \begin{bmatrix} \tilde{\mathbf{y}}_{0,0} \\ \tilde{\mathbf{y}}_{1,0} \\ \vdots \\ \tilde{\mathbf{y}}_{K-1,0} \\ \tilde{\mathbf{y}}_{0,1} \\ \vdots \\ \tilde{\mathbf{y}}_{K-2,N-1} \\ \tilde{\mathbf{y}}_{K-1,N-1} \end{bmatrix}. \tag{31}$$

The final $KNM \times 1$ delay-angle filter $\mathbf{w}(\ell, \hat{\beta})$ is comprised of down-sampled filter components in a similar manner.

In addition to the normalization in (29), a unity gain constraint for the overall delay-angle adaptive filter is enforced as

$$\mathbf{w}^H\left(\ell, \hat{\beta}\right) \left(\bar{\mathbf{g}}\left(\hat{\beta}\right) \otimes \mathbf{v}_{\hat{\beta}} \right) = 1. \tag{32}$$

Noting that (32) could be expressed as the sum of K down-

sampled components, the constraint is incorporated as a Lagrange multiplier into the cost function of (26) as

$$\tilde{J}\left(\ell,\hat{\beta}\right)=\sum_{k=0}^{K-1}E\left[\left|\frac{1}{K}\bar{x}\left(\ell,\hat{\beta}\right)-\tilde{\mathbf{w}}_k^H\left(\ell,\hat{\beta}\right)\tilde{\mathbf{y}}_k\left(\ell\right)\right|^2\right] + \mathrm{Re}\left\{\lambda\left(\sum_{k=0}^{K-1}\left(\tilde{\mathbf{w}}_k^H\left(\ell,\hat{\beta}\right)\left(\tilde{\tilde{\mathbf{g}}}_k\left(\hat{\beta}\right)\otimes\mathbf{v}_{\hat{\beta}}\right)\right)-1\right)\right\} \quad (33)$$

where λ is the Lagrange multiplier, $\mathrm{Re}\{\bullet\}$ denotes the real part of the argument, and $\tilde{\tilde{\mathbf{g}}}_k(\beta)$ is the kth length-N down-sampled version of the normalized far-field emission $\bar{\mathbf{g}}(\beta)$.

Minimization of (33) with respect to $\tilde{\mathbf{w}}_k^*(\ell,\hat{\beta})$ yields

$$\tilde{\mathbf{w}}_k\left(\ell,\hat{\beta}\right)=\left(E\left[\tilde{\mathbf{y}}_k\left(\ell\right)\tilde{\mathbf{y}}_k{}^H\left(\ell\right)\right]\right)^{-1} \times\left(\frac{1}{K}E\left[\bar{x}^*\left(\ell,\hat{\beta}\right)\,\tilde{\mathbf{y}}_k\left(\ell\right)\right]-\frac{\lambda}{2}\left(\tilde{\tilde{\mathbf{g}}}_k\left(\hat{\beta}\right)\otimes\mathbf{v}_{\hat{\beta}}\right)\right). \quad (34)$$

Assuming the delay-angle cells are uncorrelated with one another and with the noise, the filter in (34) simplifies to

$$\tilde{\mathbf{w}}_k\left(\ell,\hat{\beta}\right)=\left(\sum_{\phi}\left(\tilde{\tilde{\mathbf{G}}}_k\left(\ell,\phi\right)\otimes\mathbf{v}_\phi\mathbf{v}_\phi^H\right)+\tilde{\mathbf{R}}_k(\ell)\right)^{-1} \times\left(\frac{1}{K}\rho\left(\ell,\hat{\beta}\right)-\frac{\lambda}{2}\right)\left(\tilde{\tilde{\mathbf{g}}}_k\left(\hat{\beta}\right)\otimes\mathbf{v}_{\hat{\beta}}\right) \quad (35)$$

where $\rho(\ell,\hat{\beta})=E[|\bar{x}(\ell,\hat{\beta})|^2]$ is the expected power in the emission-normalized delay-angle cell corresponding to delay ℓ and electrical angle $\hat{\beta}$, and $\tilde{\mathbf{R}}_k(\ell)$ is the kth $NM\times NM$ down-sampled noise covariance matrix, which can be simplified assuming white noise to $\tilde{\mathbf{R}}_k(\ell)=\tilde{\mathbf{R}}_k=\sigma_u^2\mathbf{I}_{NM\times NM}$ for noise power σ_u^2. The term

$$\tilde{\tilde{\mathbf{G}}}_k\left(\ell,\phi\right)=\sum_{\tau=-KN+1}^{KN-1}\rho\left(\ell+\tau,\phi\right)\tilde{\tilde{\mathbf{g}}}_{k,\tau}(\phi)\,\tilde{\tilde{\mathbf{g}}}_{k,\tau}^H(\phi) \quad (36)$$

is the kth $N\times N$ structured signal covariance matrix where the $N\times 1$ vector $\tilde{\tilde{\mathbf{g}}}_{k,\tau}(\phi)$ is a τ delay-shifted (and zero-padded) version of the normalized and down-sampled far-field emission as

$$\tilde{\tilde{\mathbf{g}}}_{k,\tau}(\phi)= \begin{cases}\left[\bar{g}_{k-\tau}(\phi)\;\bar{g}_{k-\tau+K}(\phi)\cdots\bar{g}_{k-\tau+K\left(N-1-\tilde{\tau}\right)}(\phi)\;\mathbf{0}_{1\times\tilde{\tau}}\right]^T & \text{for } \tau\le 0\\ \left[\mathbf{0}_{1\times\tilde{\tau}}\;\bar{g}_{k-\tau+K\tilde{\tau}}(\phi)\;\bar{g}_{k-\tau+K\left(\tilde{\tau}+1\right)}(\phi)\cdots\bar{g}_{k-\tau+K(N-1)}(\phi)\right]^T & \text{for } \tau>0\end{cases} \quad (37)$$

with the down-sampled delay factor

$$\tilde{\tau}=\begin{cases}\left\lfloor\dfrac{k-\tau}{K}\right\rfloor & \text{for}\quad \tau\le 0\\ \left\lfloor\dfrac{K-1-(k-\tau)}{K}\right\rfloor & \text{for}\quad \tau>0\end{cases} \quad (38)$$

and $\lfloor\bullet\rfloor$ the floor operation.

An additional modification is administered to (36) in which, specifically for determination of the $(\ell,\hat{\beta})$ filter, a portion of the surrounding delay-angle indices are set to zero. This modification, previously used for optimal mismatched filtering [8] actually reduces the degree of super-resolution in delay and angle. It thus has the benefit of greatly reducing straddling effects in both dimensions and thereby mitigating the ensuing mismatch loss (i.e. "off-grid" effects).

The surrounding region for zero-filling is defined as

$$\rho\left(\ell_{\text{beam}},\hat{\beta}_{\text{beam}}\right)=\begin{cases}\rho\left(\ell,\hat{\beta}\right) & \text{if } \ell_{\text{beam}}=\ell \text{ and } \hat{\beta}_{\text{beam}}=\hat{\beta}\\ 0 & \text{otherwise}\end{cases} \quad (39)$$

for

$$\ell_{\text{beam}}\in\left[\ell-\ell_{\text{BW}},\ell+\ell_{\text{BW}}\right] \text{ and } \hat{\beta}_{\text{beam}}\in\left[\hat{\beta}-\hat{\beta}_{\text{BW}},\hat{\beta}+\hat{\beta}_{\text{BW}}\right], \quad (40)$$

where ℓ_{BW} and $\hat{\beta}_{\text{BW}}$ specify the peak-to-null beamwidths in the range and electrical angle after adaptive processing.

The Lagrange multiplier from (35) is, as usual, determined by evaluating the constraint, which in this case becomes

$$\sum_{i=0}^{K-1}\tilde{\mathbf{w}}_i{}^H\left(\ell,\hat{\beta}\right)\left(\tilde{\tilde{\mathbf{g}}}_i\left(\hat{\beta}\right)\otimes\mathbf{v}_{\hat{\beta}}\right)= \sum_{i=0}^{K-1}\left(\frac{1}{K}\rho\left(\ell,\hat{\beta}\right)-\frac{\lambda}{2}\right)\times \left(\tilde{\tilde{\mathbf{g}}}_i\left(\hat{\beta}\right)\otimes\mathbf{v}_{\hat{\beta}}\right)^H\left(\sum_{\phi}\left(\tilde{\tilde{\mathbf{G}}}_i(\ell,\phi)\otimes\mathbf{v}_\phi\mathbf{v}_\phi^H\right)+\tilde{\mathbf{R}}_i\right)^{-1}\left(\tilde{\tilde{\mathbf{g}}}_i\left(\hat{\beta}\right)\otimes\mathbf{v}_{\hat{\beta}}\right) \quad (41)$$

Subsequently solving for λ results in

$$\frac{\lambda}{2}=\frac{1}{K}\rho(\ell,\hat{\beta})\;- \frac{1}{\sum_{i=0}^{K-1}\left(\tilde{\tilde{\mathbf{g}}}_i\left(\hat{\beta}\right)\otimes\mathbf{v}_{\hat{\beta}}\right)^H\left(\sum_{\phi}\left(\tilde{\tilde{\mathbf{G}}}_i(\ell,\phi)\otimes\mathbf{v}_\phi\mathbf{v}_\phi^H\right)+\tilde{\mathbf{R}}_i\right)^{-1}\left(\tilde{\tilde{\mathbf{g}}}_i\left(\hat{\beta}\right)\otimes\mathbf{v}_{\hat{\beta}}\right)} \quad (42)$$

such that the SRAP filter takes the familiar MVDR-like form

$$\tilde{\mathbf{w}}_k\left(\ell,\hat{\beta}\right)= \frac{\left(\sum_{\phi}\left(\tilde{\tilde{\mathbf{G}}}_k(\ell,\phi)\otimes\mathbf{v}_\phi\mathbf{v}_\phi^H\right)+\tilde{\mathbf{R}}_k\right)^{-1}\left(\tilde{\tilde{\mathbf{g}}}_k\left(\hat{\beta}\right)\otimes\mathbf{v}_{\hat{\beta}}\right)}{\sum_{i=0}^{K-1}\left(\tilde{\tilde{\mathbf{g}}}_i\left(\hat{\beta}\right)\otimes\mathbf{v}_{\hat{\beta}}\right)^H\left(\sum_{\phi}\left(\tilde{\tilde{\mathbf{G}}}_i(\ell,\phi)\otimes\mathbf{v}_\phi\mathbf{v}_\phi^H\right)+\tilde{\mathbf{R}}_i\right)^{-1}\left(\tilde{\tilde{\mathbf{g}}}_i\left(\hat{\beta}\right)\otimes\mathbf{v}_{\hat{\beta}}\right)}. \quad (43)$$

Clearly (43) is a function of $\bar{x}(\ell,\hat{\beta})$ and the surrounding delay-angle cells, the very values it is intended to estimate. Thus a bootstrapping implementation is needed.

C. SRAP Implementation

Like its predecessors [20,22,27], SRAP relies on the RMMSE structure involving alternating estimation of the delay-angle specific filters and the delay-angle scattering coefficients (inclusive of illumination scaling), in this regard philosophically similar to the implementation of expectation-maximization [31]. Thus an initial scattering estimate is required that can be obtained by applying the delay-angle coupled matched filter from (23). The expected delay-angle cell powers therefore become the current estimates

$$\hat{\rho}(\ell,\bar{\beta}) = |\,\hat{\bar{x}}(\ell,\bar{\beta})|^2 \tag{44}$$

for use in determination of the updated filters, that then subsequently update the scattering estimates. Each iteration enhances target visibility and generally after 3 or 4 iterations no further improvement is realized. The implementation procedure is delineated in Table I. Per iteration, the computational cost of SRAP is $O((NM)^3)$ for the estimation of each range-angle cell.

TABLE I
IMPLEMENTATION OF SRAP ALGORITHM

1.	Collect KN range samples corresponding to range index ℓ over M antenna elements and arrange into $KNM\times 1$ vector $\mathbf{y}(\ell)$.
2.	Obtain initial range-angle profile estimate $\hat{\bar{x}}_{\mathrm{MF}}(\ell,\beta)$ via (23) and (24).
3.	Compute power estimates $\hat{\rho}(\ell,\bar{\beta}) = \|\hat{\bar{x}}(\ell,\bar{\beta})\|^2$ and use to calculate the K down-sampled structured covariance matrices, $\tilde{\bar{\mathbf{G}}}_k(\ell,\phi)$ for k = 0, 1, … , K-1, for all ϕ using (36) - (38) while implementing the zero-filling constraint for $\hat{\rho}(\ell,\bar{\beta})$ described in (39) and (40).
4.	Find the K down-sampled SRAP filters, $\tilde{\mathbf{w}}_k(\ell,\bar{\beta})$ for k = 0, … , K-1, for all $\bar{\beta}$ using (43) (or (45) - (48) if in eclipsed region).
5.	Interleave the down-sampled filters, $\tilde{\mathbf{w}}_k(\ell,\bar{\beta})$ for k = 0, … , K-1, for each value of $\bar{\beta}$ using the structure shown in (30) and (31) to obtain the range-angle SRAP filters $\mathbf{w}(\ell,\bar{\beta})$.
6.	Apply the SRAP filters to the data vector $\mathbf{y}(\ell)$ to obtain the updated range-angle profile estimate $\bar{x}(\ell,\bar{\beta}) = \mathbf{w}^H(\ell,\bar{\beta})\mathbf{y}(\ell)$.
7.	Go to step 3 until convergence or desired suppression is achieved.

Estimation of the scattering in the pulse-eclipsed regions [19,32] has become an integral part of the previous APC algorithm since doing so provides visibility of more of the illuminated region and thereby enhances overall estimation accuracy. To incorporate estimation of the eclipsed scattering into SRAP denote the delay indices corresponding to the non-eclipsed receive interval as $\ell = 0, 1, \cdots, Q-1$, so that $\ell < 0$ and $\ell > Q-1$ correspond to eclipsed range indices. Using (43) and [19, Chap. 8], the eclipsed region delay-angle filters can thus be defined as

$$\tilde{\mathbf{w}}_k(\ell=-q,\bar{\beta}) = \frac{\left(\dfrac{\left\|\bar{\mathbf{g}}_{-q}(\bar{\beta})\right\|}{\left\|\bar{\mathbf{g}}(\bar{\beta})\right\|}\right)\left(\sum_{\phi}\left(\tilde{\bar{\mathbf{G}}}_k^{(\ell)}(0,\phi)\otimes\mathbf{v}_\phi\mathbf{v}_\phi^H\right)+\tilde{\mathbf{R}}_k\right)^{-1}\left(\tilde{\bar{\mathbf{g}}}_{k,-q}(\bar{\beta})\otimes\mathbf{v}_{\bar{\beta}}\right)}{\sum_{i=0}^{K-1}\left(\tilde{\bar{\mathbf{g}}}_{i,-q}(\bar{\beta})\otimes\mathbf{v}_{\bar{\beta}}\right)^H\left(\sum_{\phi}\left(\tilde{\bar{\mathbf{G}}}_i^{(\ell)}(0,\phi)\otimes\mathbf{v}_\phi\mathbf{v}_\phi^H\right)+\tilde{\mathbf{R}}_i\right)^{-1}\left(\tilde{\bar{\mathbf{g}}}_{i,-q}(\bar{\beta})\otimes\mathbf{v}_{\bar{\beta}}\right)} \tag{45}$$

for the $q = 1, 2, \cdots, KN-1$ "early" eclipsed delay indices and

$$\tilde{\mathbf{w}}_k\left(\ell=Q-1+q,\bar{\beta}\right) = \frac{\left(\dfrac{\left\|\bar{\mathbf{g}}_{q}(\bar{\beta})\right\|}{\left\|\bar{\mathbf{g}}(\bar{\beta})\right\|}\right)\left(\sum_{\phi}\left(\tilde{\bar{\mathbf{G}}}_k^{(\ell)}(Q-1,\phi)\otimes\mathbf{v}_\phi\mathbf{v}_\phi^H\right)+\tilde{\mathbf{R}}_k\right)^{-1}\left(\tilde{\bar{\mathbf{g}}}_{k,q}(\bar{\beta})\otimes\mathbf{v}_{\bar{\beta}}\right)}{\sum_{i=0}^{K-1}\left(\tilde{\bar{\mathbf{g}}}_{i,q}(\bar{\beta})\otimes\mathbf{v}_{\bar{\beta}}\right)^H\left(\sum_{\phi}\left(\tilde{\bar{\mathbf{G}}}_i^{(\ell)}(Q-1,\phi)\otimes\mathbf{v}_\phi\mathbf{v}_\phi^H\right)+\tilde{\mathbf{R}}_i\right)^{-1}\left(\tilde{\bar{\mathbf{g}}}_{i,q}(\bar{\beta})\otimes\mathbf{v}_{\bar{\beta}}\right)} \tag{46}$$

for the $q = 1, 2, \cdots, KN-1$ "late" eclipsed delay indices, where $\tilde{\bar{\mathbf{g}}}_{k,-q}(\bar{\beta})$ and $\tilde{\bar{\mathbf{g}}}_{k,q}(\bar{\beta})$ have the delay-shift structure of (37). The terms in the ratios at the front of (44) and (45) are defined as

$$\left\|\bar{\mathbf{g}}_q(\bar{\beta})\right\| = \left(\sum_{k=0}^{K-1}\left\|\tilde{\bar{\mathbf{g}}}_{k,q}(\bar{\beta})\right\|^2\right)^{1/2} \tag{47}$$

$$\left\|\bar{\mathbf{g}}_{-q}(\bar{\beta})\right\| = \left(\sum_{k=0}^{K-1}\left\|\tilde{\bar{\mathbf{g}}}_{k,-q}(\bar{\beta})\right\|^2\right)^{1/2}, \tag{48}$$

to prevent over-compensation by the previous gain-constraint of (32) when an eclipsed echo is present. The superscript $(\bullet)^{(\ell)}$ in (45) and (46) signifies that the delay-angle indices that are zeroed (via (39) and (40)) surround the particular eclipsed range index under consideration and not $\ell = 0$ as in (45) or $\ell = Q-1$ as in (46). The eclipsed delay-angle filters of (45) and (46) are applied to the portions of the received signal indexed as $\mathbf{y}(0)$ and $\mathbf{y}(Q-1)$, respectively.

IV. SIMULATION OF PHYSICAL EMISSIONS & PROCESSING

Using the physical emission structure described in Section II the utility of adaptive receive processing is demonstrated. We consider a length $N = 20$ code $\mathbf{x}_{\mathrm{w}}$ that realizes a commensurate time-bandwidth product when implemented as a continuous waveform via (3). The phase-change values of $\mathbf{x}_{\mathrm{w}}$ are randomly generated from a uniform distribution on $[-\pi, \pi]$. For an array of $M = 10$ elements with half-wavelength spacing and $\theta_{\mathrm{C}} = 0°$ (i.e. boresight), the spatial code $\mathbf{x}_{\mathrm{s}}$ is defined such that the beam steers linearly (in the spatial domain) from first null to first null (Fig. 2), where the first nulls lie at electrical angles $\pm 36°$. As one would expect, the resulting emission has poor autocorrelation properties in the range domain, but serves to highlight the sidelobe

suppression capabilities of SRAP.

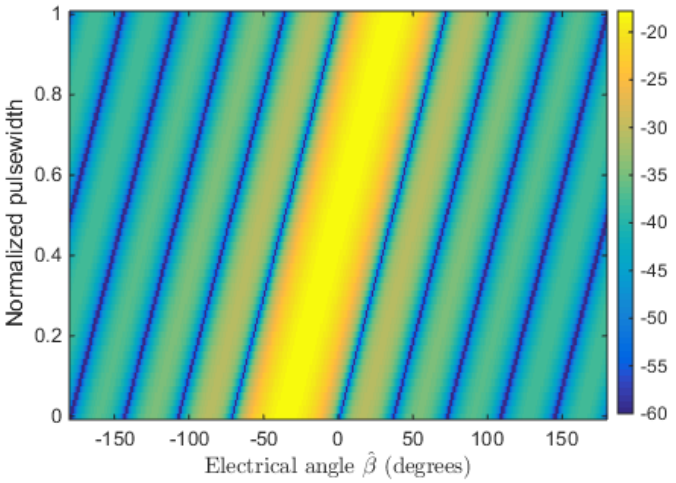

Fig. 2. Time-varying beampattern (TVBP) of a first null to first null steered beam with *M*=10 elements.

Using this physically realizable emission, we shall consider various scenarios of scatterers in noise in the absence of clutter (e.g. moving targets after Doppler clutter cancellation). The receive data are processed using the SRAP algorithm as described in Table I. For this first scenario, consider a single point scatterer at range index 30, angle $\bar{\beta} = 0°$, and an ideal SNR of 25 dB after all coherent integration (pulse compression, standard focused beamforming, and prior Doppler processing). The noise is additive white Gaussian with power 0 dB (after integration). The "over-sampling" factor is $K = 3$ for the emission and the spatial domain is partitioned on a $2°$ electrical angle grid.

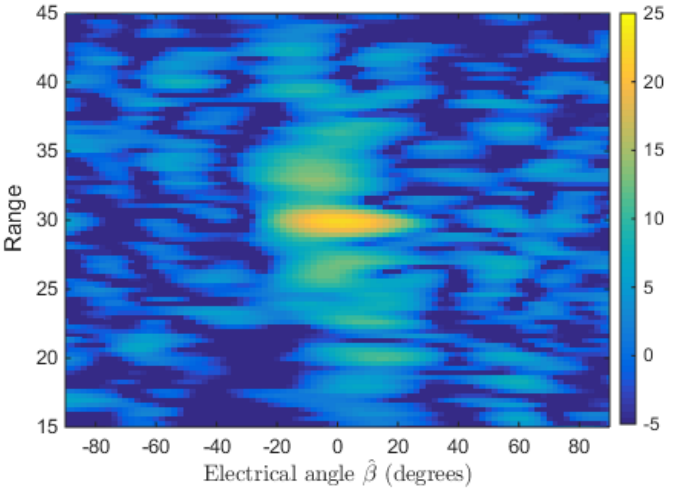

Fig. 3. Delay-angle matched filter response for a single scatterer. No delay or angle straddling. Target peak power is 22.6 dB (2.4 dB loss relative to standard beamforming)

Figures 3 and 4 show the delay-angle matched filter response and the SRAP estimate after 2 adaptive iterations (following initial matched filtering), respectively. This case involved no straddling in delay or angle (i.e. on grid) and employing no zeroing of the surrounding delay-angle cells via (36). The SRAP response is clearly superior with regard to determination of scatterer location in both delay and angle, and also provides complete suppression of surrounding sidelobes. Compared to the ideal 25 dB SNR (based on standard beamforming) the delay-angle matched filter for this coupled emission yields a target peak power of 22.6 dB while SRAP results in 21.7 dB, a 0.9 dB loss relative to the matched filter.

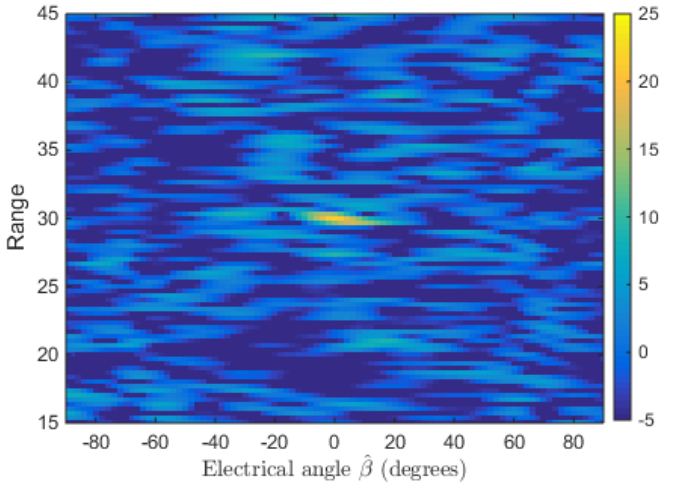

Fig. 4. SRAP response for a single scatterer. No delay or angle straddling. No delay-angle zeroing. Target peak power is 21.7 dB (3.3 dB loss relative to standard beamforming)

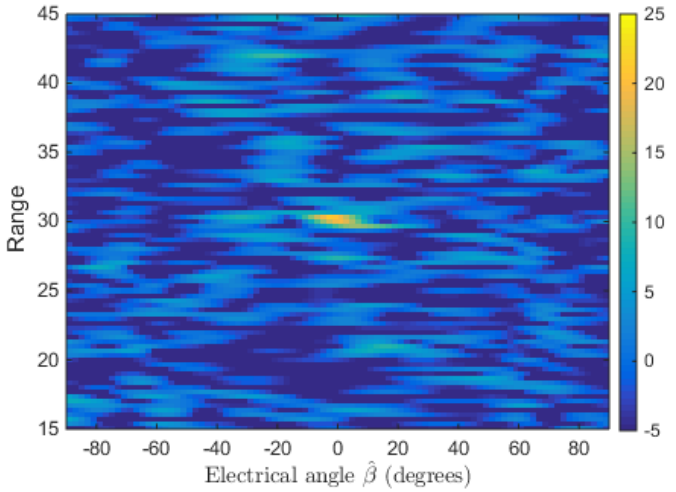

Fig. 5. SRAP response for a single scatterer. Worst-case delay and angle straddling. No delay-angle zeroing. Target peak power is 20.8 dB (4.2 dB loss relative to standard beamforming)

In contrast to the no-straddling case, Figs. 5 and 6 show the case in which the receive data has the worst-case straddling in delay for $K = 3$ and in angle for the $2°$ grid (i.e. worst-case off grid: halfway between samples). SRAP again uses 2 adaptive iterations after matched filtering. Figure 5 shows the use of SRAP without zeroing the surrounding delay-angle cells. Compared to Fig. 4, the SRAP response is now slightly blurred due to mismatch, producing an SNR of 20.8 dB, a further 0.9 dB loss relative to Fig. 4. However, by setting $\ell_{\mathrm{BW}} = K - 1 = 2$ and $\hat{\beta}_{\mathrm{BW}} = 2\pi/M = \pi/5 = 36°$ from (39) and (40) to insert surrounding zeros produces the SRAP

response in Fig. 6 in which the delay-angle resolution is now comparable to that of matched filtering with a target SNR of 22.6 dB, thus mitigating the straddling mismatch loss. The increase of SNR using the zero-filling technique shows that there exists a trade-off between enhancing resolution versus being robust to straddling effects and maximizing SNR that can be controlled by setting the amount of delay-angle "beam spoiling".

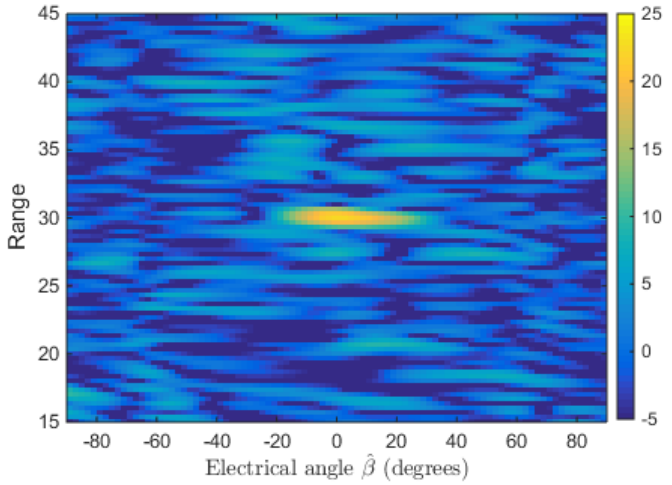

Fig. 6. SRAP response for a single scatterer. Worst-case delay and angle straddling. Delay-angle zeroing to produce nominal MF resolution. Target peak power is 22.6 dB SNR (2.4 dB loss relative to standard beamforming)

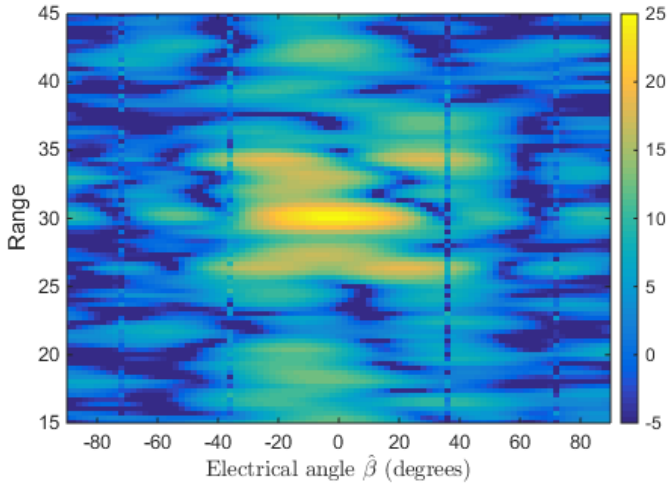

Fig. 7. Delay-angle matched filter response from standard beamforming for 5 targets in an 'X' formation.

Next consider the case of 5 targets in an 'X' pattern where two targets occupy the same range index 34 at electrical angles $\pm 25°$, a center target resides at range 30 and angle $0°$, and two more targets occupying the same range index 26 at electrical angles $\pm 25°$. All targets have an SNR of 25 dB (based on individual standard beamforming for each target) and have independent random phase. The center target exhibits no straddling (on grid) while the other 4 targets exhibit worst-case straddling in both delay and angle. For a complete comparison, both the standard emission (no spatial modulation) and that from Fig. 2 are examined. The SRAP zeroing parameters in this case are set to $\ell_{\text{BW}} = K - 1 = 2$ and $\hat{\beta}_{\text{BW}} = \pi/20 = 9°$ (4× narrower than the previous example).

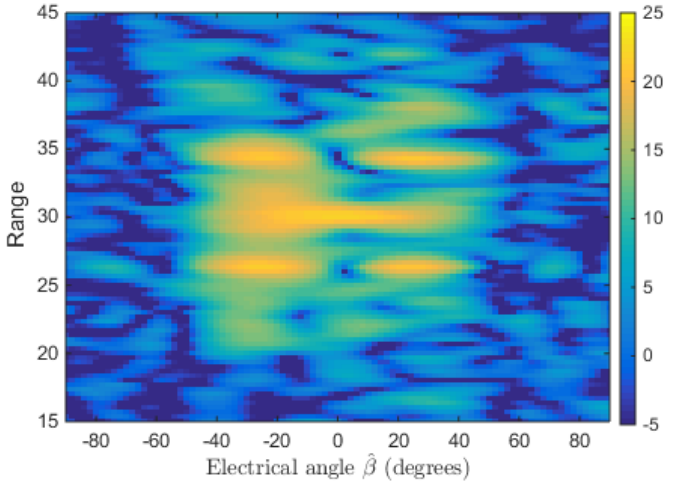

Fig. 8. Delay-angle matched filter response from spatial modulation for 5 targets in an 'X' formation.

Figures 7 and 8 depict the delay-angle matched filter responses to the standard beamforming emission and to the spatial modulation emission from Fig. 2, respectively. The former in Fig. 7 clearly shows the central target but the outer four could be characterized as ambiguous peaks. The spatial modulation case in Fig. 8, however, shows the five targets with relatively the same SNR, though their visibility is limited by the matched filter resolution capability.

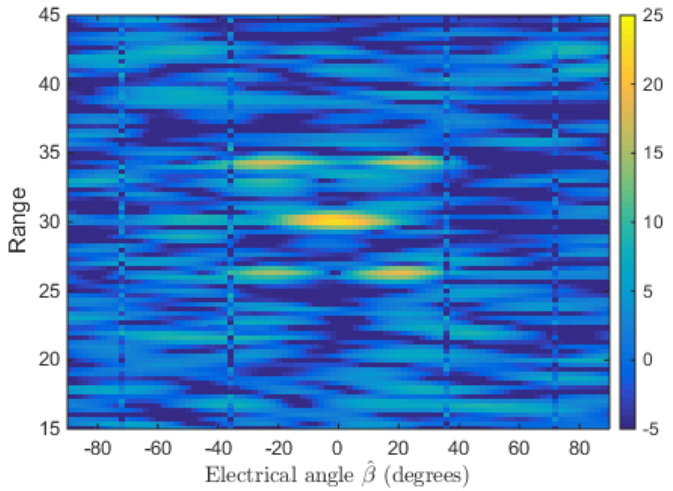

Fig. 9. SRAP response to standard beamforming for 5 targets in an 'X' formation.

Using SRAP for this same five target scenario, Fig. 9 illustrates the enhancement that is achieved after 2 iterations of the SRAP algorithm when the standard beamforming emission is employed. The five targets can now be identified, though the outer four targets again exhibit an SNR loss due to the spatially focused emission. The vertical lines that appear in Figs. 7 and 9 at angles $\pm 36°$ and $\pm 72°$ correspond to the nulls in the transmit beampattern.

In contrast Fig. 10 shows the range-angle profile after 2 iterations of SRAP with the spatial modulation emission. Now all five targets exhibit the same SNR, implying that the four outside targets do not exhibit deleterious effects after adaptive processing due to straddling.

The reduction of the parameter $\hat{\beta}_{\text{BW}}$ for Figs. 9 and 10 limit the width of the mainbeam (in the electrical domain) by a significant amount without sacrificing much mismatch loss due to delay-angle straddling. Just as the human eye behaves according to lighting conditions (i.e. SNR) it is apparent that adaptive receive processing can likewise trade some loss for enhanced acuity when SNR is sufficiently high.

The RMSE values of the 5 target locations for Figures 9 and 10 are 0.3 range cells for both cases and 3.23 and 1.73 degrees, respectively. The spatial modulation transmission scheme reduced the RMSE of the target location to almost half that of standard beamforming for this particular case. Although anecdotal, these results are encouraging.

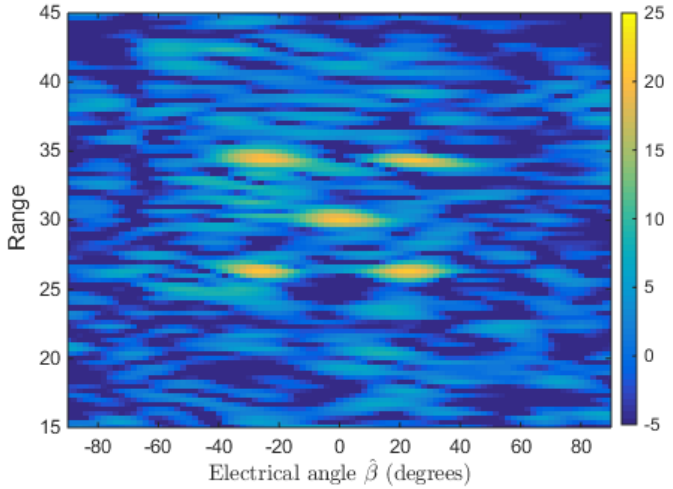

Fig. 10. SRAP response from spatial modulation for 5 targets in an 'X' formation.

Now consider a target profile containing a large target at range index 30 and angle $0°$ with an SNR of 40 dB and two smaller targets at ranges 30 and 35 and angles $36°$ and $0°$, respectively, each with an SNR of 20 dB. Recall that the stated SNR value is based on individual beamforming for each target after coherent integration (thus representing an ideal condition). The "over-sampling" factor is $K = 3$ for the emission and the spatial domain is partitioned on a $2°$ electrical angle grid. All three targets exhibit worst-case straddling in range and no straddling in angle. For this example the spatially modulated emission from Fig. 2 is once again used.

Figures 11 and 12 show the target responses of the aforementioned range-angle profile at an angle cut of $\hat{\beta} = 0°$ and range cut of 30, respectively, for four different receive processing scenarios: matched filtering and 3 SRAP scenarios with varying parameters. The parameters chosen for the different SRAP scenarios are listed in Table II.

TABLE II
SRAP PARAMETERS FOR FIGS. 11 AND 12

Case	$\hat{\beta}_{\text{BW}}$	ℓ_{BW}	Iterations
SRAP1	$\pi/5 = 36°$	K-1=2	2
SRAP2	$\pi/20 = 9°$	K-1=2	2
SRAP3	0	0	2

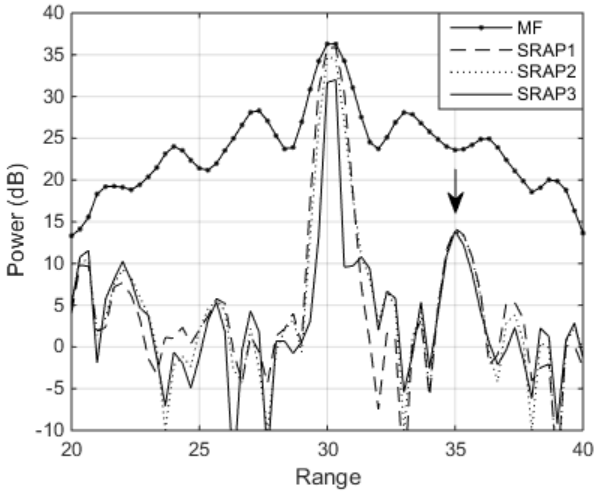

Fig. 11. $\hat{\beta} = 0°$ cut of target profile using multiple receive processing methods. Targets located at ranges 30 and 35.

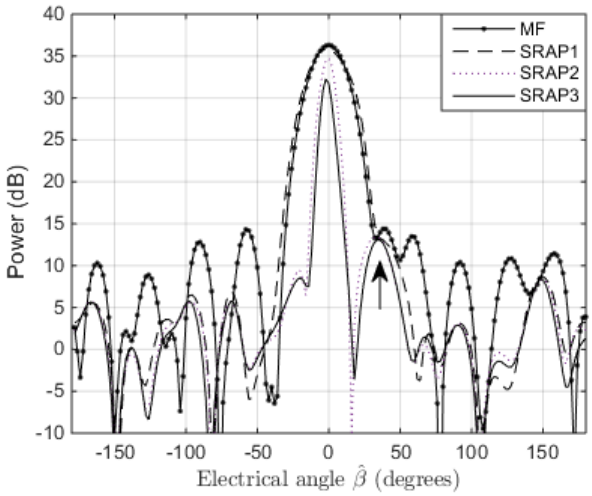

Fig. 12. Range = 30 cut of target profile using multiple receive processing methods. Targets located at $\hat{\beta} = 0°$ and $36°$.

All three scenario of SRAP suppress the sidelobes in range and angle that otherwise result from standard matched filtering beamforming. Through this suppression, the smaller target in range (identified by the black arrow) is clearly shown in all three SRAP scenarios (Fig. 11), and the smaller target in angle is revealed in SRAP cases 2 and 3 (Fig. 12). The zero-padding in angle parameterized by $\hat{\beta}_{\text{BW}}$ widens the mainlobe of SRAP case 1 to the extent that it masks the smaller target, however this is the case that exhibits the least loss on the dominant target. Table III shows the losses of the dominant target and

smaller target (when applicable) for each case. The trade-off between target loss and resolution demonstrates the ability of SRAP to adapt to the current situation.

TABLE III
TARGET PROPERTIES FOR FIGS. 11 AND 12

Case	Loss on dominant target*	Visible small target in (range/angle)?	Loss on small target in (range/angle)*
MF	3.69 dB	n/n	-/-
SRAP1	4.23 dB	y/n	5.82/- dB
SRAP2	5.27 dB	y/y	6.15/6.78 dB
SRAP3	8.31 dB	y/y	6.12/6.96 dB

* Loss compared to a standard focused beam on target

V. CONCLUSIONS

Delay-angle coupled radar emissions, often referred to as co-located MIMO, may enhance target discrimination capability much like the human eye. Using the recent demonstration of a physical implementation of a particular form of MIMO involving spatial modulation of the focused mainbeam direction in fast-time, an adaptive receive filter structure has been developed that jointly estimates the delay-angle response of the illuminated scene. It is shown that the Space-Range Adaptive Processing (SRAP) structure permits variable delay-angle resolution to account for possible straddling effects that otherwise induce mismatch loss. As such, the combination of spatially modulated emission and SRAP receive processing provide the means with which to realize a physically implementable delay-angle imaging scheme that may have possible application to various radar sensing modalities. While not considered here, fast-time Doppler for high-speed targets and/or high operating frequency could also be addressed by incorporating [33,34]. Likewise, dual-polarization effects could be addressed by incorporating the adaptive processing extension in [35].

REFERENCES

[1] S.D. Blunt, P. McCormick, T. Higgins, and M. Rangaswamy, "Spatially-modulated radar waveforms inspired by fixational eye movement," *IEEE Radar Conf.*, Cincinnati, OH, May 2014, pp. 900-905.

[2] S.D. Blunt, P. McCormick, T. Higgins, and M. Rangaswamy, "Physical emission of spatially-modulated radar," *IET Radar, Sonar & Navigation*, vol. 8, no. 12, Dec. 2014.

[3] P. Antonik, M.C. Wicks, H.D. Griffiths, and C. J. Baker, "Range-dependent beamforming using element level waveform diversity," *Intl. Waveform Diversity and Design Conf.*, Lihue, HI, Jan. 2006.

[4] P. Baizert, T.B. Hale, M.A. Temple, and M.C. Wicks, "Forward-looking radar GMTI benefits using a linear frequency diverse array," *IEE Electronics Letters*, vol. 42, no. 22, pp. 1311-1312, Oct. 2006.

[5] M. Secmen, S. Demir, A. Hizal, and T. Eker, "Frequency diverse array antenna with periodic time modulated pattern in range and angle," *IEEE Radar Conf.*, Waltham, MA, Apr. 2007, pp. 427-430.

[6] T. Higgins and S.D. Blunt, "Analysis of range-angle coupled beamforming with frequency-diverse chirps," *Intl. Waveform Diversity & Design Conf.*, Orlando, FL, Feb. 2009, pp. 140-144.

[7] P.F. Sammartino, C.J. Baker, and H.D. Griffiths, "Frequency diverse MIMO techniques for radar," *IEEE Trans. Aerospace & Electronic Systems*, vol. 49, no. 1, pp. 201-222, Jan. 2013.

[8] S.D. Blunt, M. Cook, J. Jakabosky, J. de Graaf, and E. Perrins, "Polyphase-coded FM (PCFM) waveforms: part I: implementation," *IEEE Trans. Aerospace & Electronic Systems*, vol. 50, no. 3, pp. 2218-2229, July 2014.

[9] S.D. Blunt, M. Cook, J. Jakabosky, J. de Graaf, and E. Perrins, "Polyphase-coded FM (PCFM) waveforms: part II: optimization," *IEEE Trans. Aerospace & Electronic Systems*, vol. 50, no. 3, pp. 2230-2241, July 2014.

[10] *IRIG Standard 106-00: Telemetry Standards*, Range Commanders Council Telemetry Group.

[11] *Bandwidth-Efficient Modulations: Summary of Definitions, Implementation, and Performance*, Report Concerning Space Data System Standards, Informational Report CCSDS 413.0-G-2.

[12] *Specifications of the Bluetooth System*, Bluetooth Special Interest Group, ver. 1.2, Nov. 2003.

[13] M. Rolfs, "Microsaccades: small steps on a long way," *Vision Research*, vol. 49, pp. 2415-2441, 2009.

[14] E. Ahissar and A. Arieli, "Seeing via miniature eye movements: a dynamic hypothesis for vision," *Frontiers in Computational Neuroscience*, vol. 6, no. 89, Nov. 2012.

[15] J. Cui, M. Wilke, N.K. Logothetis, D.A. Leopold, and H. Liang, "Visibility states modulate microsaccade rate and direction," *Vision Research*, vol. 49, pp. 228-236, 2009.

[16] S. Haykin, Y. Xue, and P. Setoodeh, "Cognitive radar: step toward bridging the gap between neuroscience and engineering," *Proc. IEEE*, vol. 100, no. 11, pp. 3102-3130, Nov. 2012.

[17] M. Wicks, E. Mokole, S. Blunt, R. Schneible, and V. Amuso, eds., *Principles of Waveform Diversity and Design*, SciTech, 2010.

[18] U. Pillai, K.Y. Li, I. Selesnick, and B. Himed, *Waveform Diversity: Theory & Applications*, McGraw-Hill, 2011.

[19] F. Gini, A. De Maio, and L. Patton, eds., *Waveform Design and Diversity for Advanced Radar Systems*, IET, 2012.

[20] S.D. Blunt and K. Gerlach, "Adaptive pulse compression via MMSE estimation," *IEEE Trans. Aerospace & Electronic Systems*, vol. 42, no. 2, pp. 572-584, Apr. 2006.

[21] D. Henke, P. McCormick, S.D. Blunt, and T. Higgins, "Practical aspects of optimal mismatch filtering and adaptive pulse compression for FM waveforms," *IEEE Intl. Radar Conf.*, Washington, DC, May 2015.

[22] S.D. Blunt, T. Chan, and K. Gerlach, "Robust DOA estimation: the reiterative superresolution (RISR) algorithm," *IEEE Trans. Aerospace & Electronic Systems*, vol. 47, no. 1, pp. 332-346, Jan. 2011.

[23] F. Daum and J. Huang, "MIMO radar: snake oil or good idea?" *IEEE Aerospace & Electronic Systems Mag.*, vol. 24, no. 5, pp. 8-12, May 2009.

[24] G. Frazer, Y. Abramovich, and B. Johnson, "Spatially waveform diverse radar: perspectives for high frequency OTHR", *IEEE Radar Conf.*, pp. Boston, MA, Apr. 2007, pp. 385–390.

[25] B. Cordill, J. Metcalf, S.A. Seguin, D. Chatterjee, and S.D. Blunt, "The impact of mutual coupling on MIMO radar emissions," *IEEE Intl. Conf. EM in Advanced Applications*, Sept. 2011, pp. 644-647.

[26] G. Babur, P.J. Aubry, and F. Le Chevalier, "Antenna coupling effects for space-time radar waveforms: analysis and calibration," *IEEE Trans. Antennas & Propagation*, vol. 62, no. 5, pp. 2572–2586, May 2014.

[27] T. Higgins, S.D. Blunt, and A.K. Shackelford, "Space-range adaptive processing for waveform-diverse radar imaging," *IEEE Intl. Radar Conf.*, Washington, DC, May 2010.

[28] L. Ryan, J. Jakabosky, S.D. Blunt, C. Allen, and L. Cohen, "Optimizing polyphase-coded FM waveforms within a LINC transmit architecture," *IEEE Radar Conf.*, Cincinnati, OH, May 2014, pp. 835-839.

[29] M. Popescu, S.D. Blunt, and T. Chan, "Magnetoencephalography source localization using the source affine image reconstruction (SAFFIRE) algorithm", *IEEE Trans. Biomedical Engineering*, vol. 57, no. 7, pp. 1652-1662, July 2010.

[30] S.D. Blunt and T. Higgins, "Dimensionality reduction techniques for efficient adaptive radar pulse compression," *IEEE Trans. Aerospace & Electronic Systems*, vol. 46, no. 1, pp. 349-362, Jan. 2010.

[31] T.K. Moon, "The expectation-maximization algorithm," *IEEE Signal Processing Mag.*, vol. 13, no. 6, pp. 47-60, Nov. 1996.

[32] S.D. Blunt, K. Gerlach, and E. Mokole, "Pulse compression eclipsing repair," *IEEE Radar Conf.*, Rome, Italy, May 2008.

[33] S.D. Blunt, A. Shackelford, and K. Gerlach, "Single pulse imaging," *Intl. Waveform Diversity & Design Conf.*, Lihue, HI, Jan. 2006.

[34] S.D. Blunt, A.K. Shackelford, K. Gerlach, and K.J. Smith, "Doppler compensation & single pulse imaging using adaptive pulse compression," *IEEE Trans. Aerospace & Electronic Systems*, vol. 45, no. 2, pp. 647-659, Apr. 2009.

[35] P. McCormick, J. Jakabosky, S.D. Blunt, C. Allen, and B. Himed, "Joint polarization/waveform design and adaptive receive processing," *IEEE Intl. Radar Conf.*, Washington, DC, May 2015.

Patrick M. McCormick (S'12) received his B.S. in mechanical engineering in 2008 and B.S. electrical engineering in 2013 from the University of Kansas. He is currently pursuing a Ph.D. degree in electrical engineering from the University of Kansas on radar systems and signal processing.

His research interests include adaptive receive processing and design of alternative radar transmission schemes, including spatial and polarization diverse emissions.

Thomas Higgins was born in McPherson, KS. He received his B.S., M.S., and Ph.D degrees in electrical engineering in 2005, 2007, and 2011, respectively, from the University of Kansas.

Since 2009, he has been working at the Radar Division of the Naval Research Laboratory in Washington D.C. He has worked on adaptive pulse compression, non-identical waveform signal processing, and phase-only transmit nulling. His research interests include passive radar and adaptive signal processing.

Shannon D. Blunt (S'96—M'02—SM'07) received the Ph.D. degree in electrical engineering from the University of Missouri in 2002. From 2002 to 2005 he was with the Radar Division of the Naval Research Laboratory in Washington, D.C. Since 2005 he has been with the Department of Electrical Engineering and Computer Science at the University of Kansas where he is currently a Professor and Director of the Radar Systems & Remote Sensing Lab (RSL).

In 2012 Prof. Blunt received the IEEE/AESS Nathanson Memorial Radar Award and in 2008 received the AFOSR Young Investigator Award. He has over 100 refereed journal and conference publications, 11 patents, 5 book chapters, and co-edited the book *Principles of Waveform Diversity & Design*.

He is a member of the IEEE/AESS Radar Systems Panel where he is currently Chair of the Conferences Committee. He is an Associate Editor for *IEEE Transactions on Aerospace & Electronic Systems* and is on the Editorial Board for *IET Radar, Sonar & Navigation*. He was General Chair of the 2011 *IEEE Radar Conference* in Kansas City and is a member of the program committee for the *MSS Tri-Service Radar Symposium* series. He was Chair of the NATO SET-179 research task group on "Dynamic Waveform Diversity & Design" and a member of SET-182 on "Radar Spectrum Engineering & Management" and SET-227 on "Cognitive Radar". He is a Senior Member of IEEE.

Muralidhar Rangaswamy (S'89, M'93, SM'98, F'2006) received the B.E. degree in Electronics Engineering from Bangalore University, Bangalore, India in 1985 and the M.S. and Ph.D. degrees in Electrical Engineering from Syracuse University, Syracuse, NY, in 1992. He is presently employed as the Senior Advisor for Radar Research at the RF Exploitation Branch within the Sensors Directorate of the Air Force Research Laboratory (AFRL). Prior to this he has held industrial and academic appointments.

His research interests include radar signal processing, spectrum estimation, modeling non-Gaussian interference phenomena, and statistical communication theory. He has co-authored more than 200 refereed journal and conference record papers in the areas of his research interests. Additionally, he is a contributor to 8 books and is a co-inventor on 3 U.S. patents.

Dr. Rangaswamy is the Technical Editor (Associate Editor-in-Chief) for Radar Systems in the IEEE Transactions on Aerospace and Electronic Systems (IEEE-TAES). He served as the Co-Editor-in-Chief for the Digital Signal Processing journal and on the Senior Editorial Board of the IEEE Journal of Selected Topics in Signal Processing. He was a 2 term member of the SAM technical committee the IEEE Signal Processing Society and is a member of the Radar Systems Panel (RSP) in the IEEE-AES Society. He was General Chairman of the 4th IEEE Workshop on Sensor Array and Multichannel Processing in 2006. Dr. Rangaswamy has served on the Technical Committee of the IEEE Radar Conference series in a myriad of organizational roles. He served as the Publicity Chair for the First IEEE International Conference on Waveform Diversity and Design in 2004. He was the Technical Program Chair for the 2014 IEEE Radar Conference.

He received the IEEE Warren White Radar Award in 2013, the 2013 Affiliate Societies Council Dayton (ASC-D) Outstanding Scientist and Engineer Award, the 2007 IEEE Region 1 Award, the 2006 IEEE Boston Section Distinguished Member Award, and the 2005 IEEE-AESS Fred Nathanson memorial outstanding young radar engineer award. He was elected as a Fellow of the IEEE in January 2006 with the citation "for contributions to mathematical techniques for radar space-time adaptive processing". He received the 2012 and 2005 Charles Ryan basic research award from the Sensors Directorate of AFRL, in addition to more than 40 scientific achievement awards.